Metallic Species in Mercury's Exosphere: EMMI/New Technology Telescope Observations

Alain Doressoundiram, François Leblanc, C. Foellmi, S. Erard

The Astronomical Journal, 137:3859–3863, 2009 April doi:10.1088/0004-6256/137/4/3859

METALLIC SPECIES IN MERCURY'S EXOSPHERE: EMMI/NEW TECHNOLOGY TELESCOPE OBSERVATIONS*

A. Doressoundiram[1], F. Leblanc[2], C. Foellmi[3], and S. Erard[1]
[1] LESIA, Observatoire de Paris, F-92195 Meudon Principal Cedex, France; alain.doressoundiram@obspm.fr
[2] Service d'Aéronomie, Université Versailles Saint Quentin, CNRS, France
[3] Laboratoire d'Astrophysique de l'Observatoire de Grenoble, F-38041 Grenoble Cedex 09, France
Received 2008 October 28; accepted 2009 January 13; published 2009 March 6

ABSTRACT

We performed high spectral resolution observations of Mercury's exosphere on 2005 October 30 and 31 using the European Southern Observatory-New Technology Telescope, La Silla, Chile. The large spectral range, 385–855 nm, of the spectrograph, ESO Multi-Mode Instrument, provides a unique opportunity to search for nonidentified species in Hermian's environment. In this paper, we report a tentative detection of atomic aluminum in the exosphere of Mercury. This detection should be confirmed by further observations and can be used as an upper limit for this element in Mercury's exosphere. We also estimate the upper limit for the column densities of Fe and Si exospheric atoms. Detection of Al, a refractory element, if confirmed, as well as its high exospheric abundance (between 2 and 18) with respect to Ca would suggest either an unexpected surface composition or a relation between exosphere and surface composition that is not well understood.

Key words: planets and satellites: individual (Mercury)

1. INTRODUCTION

Mercury is surrounded by a very tenuous atmosphere, with a maximum dayside density of about 10^7 atoms cm^{-3} (Broadfoot et al. 1976). This atmosphere is collisionless (i.e., the mean free path of the atoms is greater than the scale height of the atmosphere) and therefore comparable to an exosphere having the exobase coincident with the planet's surface. The existence of an atmosphere around Mercury was discovered for the first time by the Mariner 10 spectrometers that revealed three atomic elements: H, He, and O (Broadfoot et al. 1976). The presence of Na, K, and Ca was discovered later using ground-based telescopes (Potter & Morgan 1985, 1986; Bida et al. 2000).

The lifetime for the neutral species in Mercury's exosphere is governed by their interaction with the surface and their loss into the interplanetary medium, photoionization being the fastest loss mechanism. To maintain the detected exosphere, the lost atoms must be replaced by a source mechanism. Processes of endogenic and exogenic origins act to repopulate the exosphere: implantation and re-ejection of solar wind ions (in the case of H and He), impact vaporization of meteoroids and regolith (Na, O, K, Ca), photosputtering and photodesorption (Na, K), and ion sputtering (Ca, Na, K, O).

In this paper, we describe observations obtained at European Southern Observatory (ESO)-New Technology Telescope (NTT) telescope with the ESO Multi-Mode Instrument (EMMI) spectrograph (Section 2) whose large spectral range (385–855 nm) and high spectral resolution capabilities provide a unique opportunity to search for nonidentified species in Mercury's exosphere (Section 3). These results are discussed in Section 4.

2. OBSERVATIONS AND ANALYSIS

Observations of Mercury were obtained using the EMMI instrument at the 3.6 m NTT (La Silla, Chile), during the evenings of 2005 October 30 and 31. We used the REMD mode of EMMI for high-resolution echelle spectroscopy. We used the grating echelle #14 with the cross disperser #3, together with a 1 × 1 binning and a slit of 6″ length and 0″.8 width. This instrumental setup yielded a spectral resolution of 75600 at central wavelength $\lambda = 620$ nm (dispersion of ∼0.025 Å pix^{-1}) and covered the spectral range of 385–855 nm, spanned on 89 orders. The ThAr lamp was used as spectral calibration.

The observations started as soon as the sky background was low enough so that Mercury could be seen in the guider, and ended at around airmass 5 (the telescope's lowest pointing limit is 12°). That is, we acquired data from 23:30:32 to 23:48:53 UT on October 30 and between 23:35:22 and 23:54:02 on October 31. On the first night (respectively the second night), Mercury's true anomaly angle (TAA) was equal to 227° (230°), the phase angle to 66° (68°), and Mercury's diameter to 6″.2(6″.3). Mercury's heliocentric distance was equal to 0.428 AU (0.423 UA) and its heliocentric velocity was equal to −7.71 km s^{-1} (−8.07 km s^{-1}). We aligned the slit with the parallactic angle in order to alleviate the atmospheric differential refraction. Tracking mode and motion of the slit with respect to Mercury's disk was done automatically. Mercury's exosphere was scanned at 16 slit positions with 20 s exposure time, with the slit moved perpendicularly. See Table 1 for the observational circumstances.

For the data reduction, we used standard IRAF tasks of the "echelle" module. Since the telescope was very low above the horizon, the guiding of the telescope was probably not ideal. Moreover, the very high airmass introduce a significant difference in flux between individual images. This is why we decided to extract the spectra individually from each of the two-dimensional exposures, and not from their sum.

First, the multiextension FITS files were recombined into single images. We then corrected for the bias level. Using the standard star observation of the second night, we defined a trace pattern of the echelle orders across the CCD with a width as large as possible. With the standard star image, we managed to trace 89 echelle orders. Using this trace on the combined flat-field images, a master flat field has been obtained and applied

* Based on Observations carried out at the European Southern Observatory (ESO), La Sill, Chile, Programme id 076.c-0619(A).

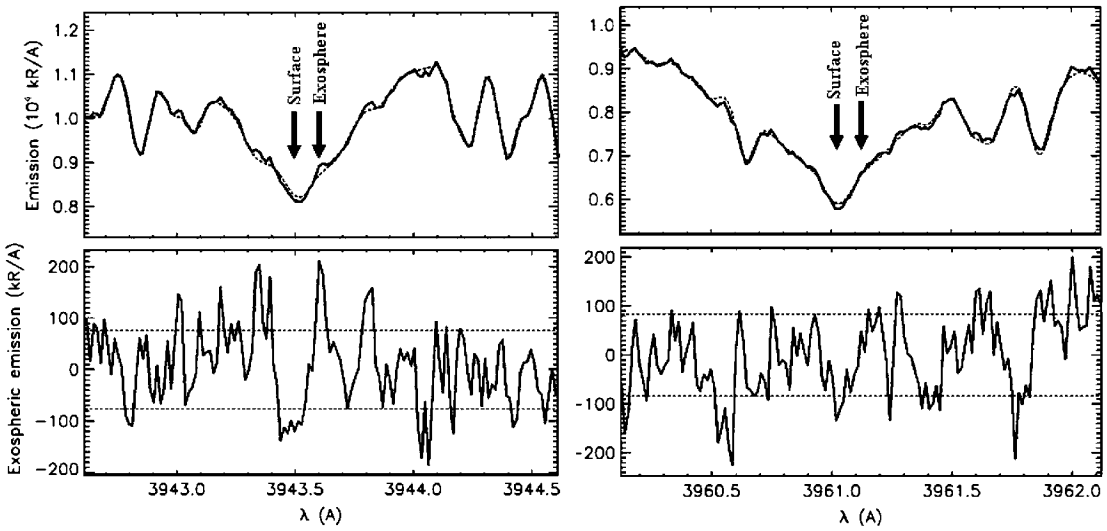

Figure 1 Spectra of the Al 3961 Å (left upper panel) and 3944 Å (right upper panel) resonant emission line as measured in Mercury's exosphere. The positions of the exospheric line and of the solar absorption line reflected at Mercury's surface as expected from ephemeris are also indicated. A solar spectrum (BASS 2000, http://bass2000.obspm.fr) has been reduced in resolution, scaled to the measured spectra and plotted in dashed line. Left and right lower panels are respectively the result of the subtraction of the measured spectra by the BASS 2000 spectrum. The dashed horizontal lines on the lower panels indicate the 1σ level.

Table 1
Observational Circumstances

UT Date	UT Start	Heliocentric Distance (AU)	Heliocentric Velocity (km s^{-1})	TAA (deg)	Phase Angle (deg)	Angular Diameter (arcsec)
2005 Oct 30	23:30:32	0.428	−7.71	227	66	6.2
2005 Oct 31	23:35:22	0.423	−8.07	230	68	6.3

to the object images. Given the EMMI instrument setup, the separation between echelle orders decreases when going toward the blue. For a pointlike object it is not a problem. However, for an elongated and very bright object such as Mercury, it makes the blue orders to overlap.

As a first consequence, we failed to extract the first four (sometimes six or seven) blue orders on some Mercury images. Those frames were discarded. For the other images, we fitted Gaussians on the horizontal cuts across the images, corresponding to the spatial profile of the orders (which are almost vertical but not perfectly, and slightly curved—this has, however, no significant influence here). Using these Gaussians, we estimate the contamination on the 5th order to be of about 50%, and rapidly decreasing.

Using the traces of extracted spectra, we obtained the corresponding Thorium–Argon calibration spectra, from images taken before the night with the exact same setup. In total, more than 400 lines were identified across the 89 echelle orders, using the atlas from La Silla Observatory completed by personal improvements since C.F. is a former La Silla Astronomer. A great care has been taken to identify the lines in the blue range. However, this task is very difficult in this domain of the spectrum given the sparse amount of lines and their weak intensities.

We also attempted a flux calibration by using a mean standard star spectrum from the second night. In order to calibrate in the flux, it was necessary to construct a one-dimensional spectrum of the standard star. For that we used the master flat to define a blaze function, which has been then divided out of the standard star spectrum. Once the orders were merged, the standard star spectrum has been used to create the sensitivity function to calibrate Mercury spectra. However, given the very high airmass of Mercury's observations, the presence of only one standard star observation, only during the second night, at a single airmass quite different from that of Mercury, we roughly estimate the flux within a factor of 2.

3. EMISSION INTENSITY MEASURED BY EMMI

All the useful single slit images have been combined to increase the signal-to-noise ratio. Figure 1 displays a portion of the spectrum measured by the EMMI during the night of October 30. Figures 1(a) and (b) are centered on the two Al resonant emissions at 3944.0060 Å and 3961.5201 Å in air (Morton 2003, 2004). These emissions are associated with electronic transition from ^2S excited state to ground state $^2P_{\frac{1}{2}}$ and $^2P_{3/2}$ for 3944.0060 Å and 3961.5201 Å, respectively. These are the strongest resonant emission lines (with respect to other Al lines) within the spectral range of EMMI (NIST database, Morton et al. 2003).

We did not subtract a sky contribution to these spectra. However the comparison between the solar spectrum (BAAS 2000), dashed line in Figure 2, and the measured emission clearly shows that the contribution of the sky to the measured emission is negligible.

Taking into account the Doppler shift of the Mercury with respect to the Sun (−7.71 km s^{-1}) and the relative velocity between the Earth and Mercury (−30.14 km s^{-1}), we have indicated the positions of the solar emission line reflected from Mercury's surface (indicated by the arrow with "Surface") and of the exospheric emission line (indicated by the arrow with "exosphere") in Figure 1. As can be seen in the left upper panel, there is a peak in the measured spectra at the expected position for the 3944.0060 Å line. Using the solar spectrum (BAAS 2000) convolved with the instrumental function to subtract the reflected light on the Mercury, it is possible to extract any potential emission lines (lower panels in Figure 1). As shown in the left lower

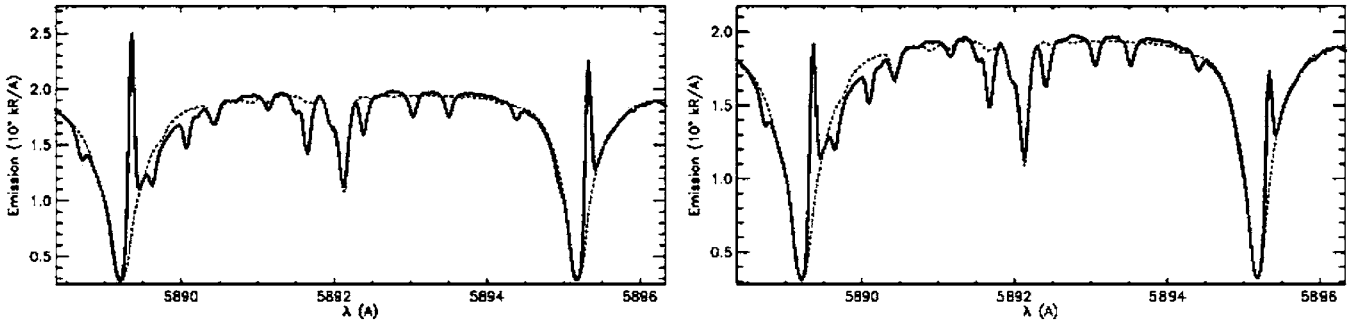

Figure 2 Spectrum measured by EMMI/NTT centered on the Na D_1 and D_2 emission lines. The positions of the exospheric line and of the solar absorption line reflected at Mercury's surface as expected from ephemeris are also indicated. A solar spectrum (BASS 2000, http://bass2000.obspm.fr) has been reduced in resolution, scaled to the measured spectra and plotted in dashed line. Left panel: measured during the night of October 30. Right panel: measured during the night of October 31.

panel, the 3944.0060 Å emission line peaked at 2.8 standard deviation (σ). There are "emission peaks" at 3943.8, 3943.35, and 3943.0 Å that are just weaker than the apparent aluminum emission peak. However, the 3943.35 and 3943.0 peaks are too narrow to be due to emission lines. The 3943.8 line appears weaker ($<2\sigma$). In contrast, we did not identify a clear emission line corresponding to the 3961.5201 Å emission line, except a small bump peaking at 1.2σ. It is still possible to integrate these two lines. We found intensities of 10.7 ± 9.1 kRayleigh (kR) and 6.0 ± 8.7 kR for the 3944.0060 Å and 3961.5201 Å, respectively. The full width at half-maximum (FWHM) of the 3944.0060 Å emission line is ~40 mÅ whereas the FWHM of the bright Na D_1 and D_2 emission lines is equal to 90 mÅ, also to be compared to the 78 mÅ instrumental resolution. Such a discrepancy might be due to the poor signal-to-noise ratio of the 3944.0060 Å emission line and to the difficulty in properly extract the emission line. It is therefore not possible to firmly conclude on the detection of the Al emission line in Mercury's exosphere. Nonetheless, the measured intensity derived from this observation can be used as an upper limit for this element in Mercury's exosphere. Moreover, if confirmed by further observations, we would like, in the following, to highlight what could be deduced on Mercury's exosphere formation from such a type of observation.

We did not observe any emission line during the second night of observation. However, when comparing the Na D_1 and D_2 emission lines for both nights (Figure 2), it can be seen that these emissions were significantly less bright during the second night when compared to the continuum. Therefore, either during the first night the exosphere of Mercury (at least its sodium component) was particularly bright or during the second night Mercury's exospheric sodium component was particularly less bright. The Na D_2 and D_1 emission brigthnesses are of 1710 ± 127 kR and 1260 ± 127, respectively, during the first night which is significantly larger than the 1110 ± 112 and 730 ± 98 kR emission brigthnesses for the second night.

Below we calculate an equivalent column density for these emission intensities under the assumption that the exosphere is optically thin. In that case, the column density N along the line of sight (in atoms cm^{-2}) is related to the emission intensity $4\Pi \times I$ in Rayleigh by the following relation $4\Pi \times I = 10^{-6} N \times g$ where g (in s^{-1}) is the photon scattering probability of Al atoms at Mercury orbit. g depends on the solar flux at the emission line calculated at Mercury's distance to the Sun and on the absorption oscillator strength. Using a high-resolution visible solar flux measured by Kurucz et al. (1984), the absorption oscillator strengths given by Morton (2003, 2004) and taking into account Mercury's Doppler shift with respect to the Sun, we have calculated g at 1 AU as being equal to 0.144 s^{-1} for the 3944.0060 Å emission line and of 0.141 s^{-1} for the 3961.5201 Å emission line. During the first night of EMMI observations, Mercury was at a heliocentric distance of 0.428 AU so that g IN the Mercury was equal to 0.786 s^{-1} for the 3944.0060 Å emission line and to 0.770 s^{-1} for the 3961.5201 Å emission line.

Therefore, we found column densities equal to $14 \pm 11 \times 10^9$ Al cm^{-2} and $7.8 \pm 11 \times 10^9$ Al cm^{-2} when calculated from the 3944.0060 Å and 3961.5201 Å emission lines, respectively.

Morgan & Killen (1997) have predicted a value for the zenith column density of 3×10^9 Al cm^{-2} which is equivalent to 4.2×10^{10} Al cm^{-2} along a tangent line of sight (Morgan and Killen regolith model) and zenith column densities 4.5×10^9 Al cm^{-2}, 1.2×10^9 Al cm^{-2}, and $1.4\ 3 \times 10^{11}$, for the volatile, intermediate, and refractory models of Goettel et al. (1988). These should be multiplied by ~14 to derive tangent column density following Morgan & Killen (1997). Knowing the present uncertainty on our measured column densities, the volatile and intermediate models theoretical numbers are in good agreement with our measured ones.

The Na D2 and D1 emission brigthnesses of the first night correspond to column densities between $7.4 \pm 0.5 \times 10^{10}$ Na cm^{-2} and $9.2 \pm 0.9 \times 10^{10}$ Na cm^{-2} which are slightly larger than the column density between 2 and 6×10^{10} Na cm^{-2} estimated by Potter et al. (2007) for a similar TAA. The Ca emission line at a wavelength of 4226.728 in air (Morton 2003) has been discovered by Bida et al. (2000) using the Keck telescope and spatially and spectrally described by Killen et al. (2005). We have looked for this emission line in the EMMI spectrum but did not succeed in identifying such an emission (Figure 3).

We can however calculate an upper limit for the intensity of this emission line. The standard deviation between solar flux and measured flux around the Ca emission line is equal to $\sigma = 64$ kR $Å^{-1}$, the FWHM of a spectral line is equal to 90 mÅ (estimated from the D2 and D1 Na emission lines, Figure 2) and therefore the integration of a Gaussian function of peak value equal to three standard deviation, and of FWHM equal to $\lambda = 90$ mÅ is equal to $3 \times \sigma \times \lambda \times \Pi^{1/2} / (2 \times (\ln(2))^{1/2}) = 19$ kR. Bida et al. (2000) reported emission intensities of few hundreds of Rayleigh. We can then calculate the g factor following the same method as previously and derive a g factor equal to 13.35 s^{-1}. Therefore the upper limit for the column density of Ca atoms is equal to 1.4×10^9 Ca cm^{-2}. Bida et al. (2000) measured the column density between 3.67×10^7 Ca

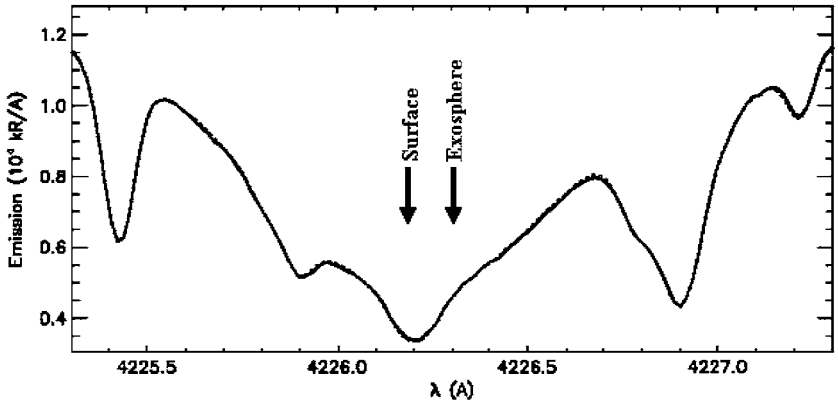

Figure 3 Spectrum measured by EMMI/NTT centered on the Ca 4227 Å emission line. The positions of the exospheric line and of the solar absorption line reflected at Mercury's surface as expected from ephemeris are also indicated. A solar spectrum (BASS 2000, http://bass2000.obspm.fr) has been reduced in resolution, scaled to the measured spectra and plotted in dashed line.

Table 2
Abundances

Species	Line (Å)	g-factor s^{-1}	Intensity (kR)	Column Density (atoms cm^{-2})
Al	3944.0060	0.786	<10.7[a]	$<14 \times 10^9$
Al	3961.5201	0.770	<6.0[a]	$<7.8 \times 10^9$
Na D_2	5889.9510	23.13	1710±127[a]	$7.4 \pm 0.5 \times 10^{10}$
Na D_1	5895.9242	13.74	1260±127[a]	$9.2 \pm 0.9 \times 10^{10}$
Ca	4226.728	13.35	<19[a]	$<1.4 \times 10^9$
Fe	3920.2578	0.170	<18[b]	$<1 \times 10^{11}$ Fe
Li	6707.761	56.38	<6[b]	$<4 \times 10^7$
	6707.912	84.64		
	6708.072	28.27		
Si	3906.629	0.31	<16[b]	$<5 \times 10^{10}$

Notes.
[a] First night.
[b] Average on both nights.

cm^{-2} and 1.8×10^8 Ca cm^{-2} (Bida et al. 2000) corresponding to an average zenith column density equal to 1.1×10^8 Ca cm^{-2}, in good agreement with Killen et al. (2005).

In the same way, we can derive upper limits for the column density of Fe at 3920 Å, of Li at 6708 Å and of Si at 3906 Å during the first night. We found an upper limit for the emission brightness of these emission lines of 31, 8, and 27 kR for Fe at 3920 Å, Li at 6708 Å, and Si at 3906 Å, respectively (and of 18 kR, 6 kR, and 16 kR when we average all spectra of both nights). These emission lines correspond then to upper limits of 2×10^{11} Fe cm^{-2}, 5×10^7 Li cm^{-2} and 8×10^{10} Si cm^{-2} tangent column densities in Mercury's exosphere during the first night of observation (to 1×10^{11} Fe cm^{-2}, 4×10^7 Li cm^{-2}, and 5×10^{10} Si cm^{-2} in an average during both nights).

4. DISCUSSION AND CONCLUSION

Our EMMI observations led to the marginal detection of Al exospheric lines both at 3944.0060 Å and 3961.5201. This detection should be confirmed by further observations and can be used as an upper limit for this element in Mercury's exosphere.

If confirmed by further observations, using the lower bound of the column density for the aluminum measured by the EMMI and the upper limit on the Ca column density, we would therefore be left with a ratio between aluminum and calcium between 2 and 18. Since both aluminum and calcium are refractory species, it is most probable that they are ejected from Mercury's surface by energetic processes such as ion sputtering or meteoritic vaporization. Both these processes are efficient and roughly stoichiometric with respect to the relative abundance in Mercury's upper surface. Starting from a regolith composition close to that suggested by Morgan & Killen (1997), that is with a regolith enriched in aluminum by less than 70% larger with respect to Ca, Johnson & Baragiola (1991) calculated a ratio of 4 between the Al and Ca exospheric abundances. This was derived using Hapke formulation of regolith sticking, ballistic lifetime, and ionization loss. In this model, the difference in mass is large enough to enrich the exosphere of the Moon in Al with respect to Ca which implies that a similar ratio would be found at the Mercury. This model also predicted an abundance in Si (which is also a refractory specie) six times larger than that of Ca which is therefore also in agreement with our upper limit for this specie, 5×10^{10} Si cm^{-2}. We also confirm the upper limits set by Sprague et al. (1996) for the Li abundance in Mercury's exosphere as being smaller than 4×10^7 Li cm^{-2} and provide the first upper limit for the exospheric iron as 10^{11} Fe cm^{-2} (see Table 2). The iron upper limit is interesting by the fact that Mercury surface is known to be depleted in ferrous iron (Vilas 1985). The content of Fe in the exosphere could possibly *constrain*, once the source processes are clearly understood, the regolith's composition. This could in turn permit to distinguish between differents scenario formations (Goettel et al. 1988). The Mercury Atmospheric and Surface Composition Spectrometer (MASCS) onboard the MESSENGER spacecraft, should be

able to detect Fe exospheric line at 3719 Å, as well as many other species in the 115–600 nm spectral range (McClintock & Lankton 2007).

However, this increase from surface to exosphere is not enough to reconcile our marginal measurements of Al with the typical column density for the Ca measured by Bida et al. (2000). Therefore, either the real abundance of Al in Mercury's exosphere is significantly below the values derived here, or the main sources of Ca and Al exospheric atoms are either not similar and in any case not stoichiometric with respect to the surface. In that later case, the value of the column density of Al in Mercury's exosphere derived from our marginal identification would suggest that either Ca or Al is not produced stoichiometrically from the surface into the exosphere or that the surface of Mercury should be significantly enriched in Al with respect to Ca.

At the end, the presence of any atomic Al species in Mercury's exosphere should be associated with a population of Al^+ ions since the photo-ionization lifetime of an Al atom at Mercury distance to the Sun is typically of less than 5 minutes (Fulle et al. 2007). During its first flyby of Mercury, MESSENGER did not report the detection of such ionic species (Zurbuchen et al. 2008), even if their Figure 1 might suggest the existence of a population at the mass 27.

We thank R.E Johnson and E. Lellouch for helpful comments on this paper during its preparation.

REFERENCES

Bida, T. A., Killen, R. M., & Morgan, T. H. 2000, Nature, 404, 159
Broadfoot, A. L., Shemansky, D. E., & Kumar, S. 1976, Geophys. Res. Lett., 3, 577
Fulle, M., et al. 2007, ApJ, 661, L93
Goettel, K. A. 1988, in Mercury, ed. F. Vilas, C. Chapman, & M. Matthews (Tucson, AZ: Univ. Arizona Press), 613
Johnson, R. E., & Baragiola, R. 1991, Geophys. Res. Lett., 18, 2169
Killen, R. M., Bida, T. A., & Morgan, T. H. 2005, Icarus, 173, 300
Kurucz, I. F., Brault, J., & Testerman, L. 1984, National Solar Observatory Atlas No. 1 (Sunspot, NM: National Solar Observatory) NSO/Kitt Peak FTS data used here were produced by NSF/NOAO
McClintock, W. E., & Lankton, M. R. 2007, Space Sci. Rev., 131, 481
Morgan, T. H., & Killen, R. M. 1997, Planet. Space Sci., 45, 81
Morton, D. C. 2003, ApJS, 149, 205
Morton, D. C. 2004, ApJS, 151, 403
Potter, A. E., Killen, R. M., & Morgan, T. H. 2007, Icarus, 186, 571
Potter, A. E., & Morgan, T. H. 1985, Science, 229, 651
Potter, A. E., & Morgan, T. H. 1986, Icarus, 67, 336
Sprague, A. L., Hunten, D. M., & Grosse, F. A. 1996, Icarus, 123, 345
Vilas, F. 1985, Icarus, 64, 133
Zurbuchen, T. H., et al. 2008, Science, 321, 90